Research Article

Synthesis of activated carbon from olive seeds: investigating the yield, energy efficiency, and dye removal capacity

Oluranti Agboola[1] · Benjamin Okoli[1] · Samuel E. Sanni[1] · Peter Adeniyi Alaba[1] · Patricia Popoola[2] · Emmanuel R. Sadiku[2] · Patrick M. Mubiayi[3] · Esther Titilayo Akinlabi[4] · Mamookho Elizabeth Makhatha[5]

Abstract
This study explored the synthesis of activated carbon from olive seeds by chemical and thermal activation, and evaluated the energy efficiency of the process. The oilseed samples were carbonized at varying temperature (600–840 °C). The produced activated carbons were used for dye removal, studying the effect of temperature. The materials were analyzed using X-ray diffraction and scanning electron microscopy (SEM). The pores and interpore spacing porous of the activated carbons were identified from the SEM images using ImageJ software. The results show that the yield of activated carbon and energy efficiency significantly decreased with increasing carbonization temperature. This reveals that a higher yield of activated carbon and higher energy efficiency was attained at lower carbonization temperature, meaning that producing activated carbon from olive seed is cost effective. Moreover, the activated carbon obtained at 600 °C exhibits the optimum removal efficiency for methylene blue, however, the increase in the removal efficiency upon increasing the temperature from 600 to 720 °C is insignificant (about 1%).

Keywords Activated carbon · Energy efficiency · Olive seeds · Dye removal · Methylene blue

1 Introduction

Different kinds of carbonaceous materials like coal, biomasses and their wastes, and some polymers have been utilized as a precursor for the synthesis of activated carbons (ACs) [1]. This is because of their outstanding performance in several process applications such as coffee decaffeination [2], water treatment [3], deodorization [4], decolorization [5], filters for cleaning air conditions [6]; Hence, ACs are occasionally referred to as "material of the future" [7]. They principally have favorable characteristics for adsorption processes because of their large surface area, high porosity, ease of compaction into a packed bed and high surface reactivity [7]. The exceptional adsorptive properties of ACs are influenced by its porosity, these properties are usually articulated to their characteristic pore distribution pattern and internal surface area. AC porosity is primarily subject to its versatile production process, which is intensely influenced by process parameters like rate of reaction by the activation agent, residence time and the and activation temperature [8]. ACs could be produced using physical or chemical treatment process. Physical treatment comprises

Electronic supplementary material The online version of this article (https://doi.org/10.1007/s42452-018-0089-5) contains supplementary material, which is available to authorized users.

✉ Oluranti Agboola, funmi2406@gmail.com; ✉ Peter Adeniyi Alaba, adeniyipee@live.com | [1]Department of Chemical Engineering, Covenant University, Ota, Nigeria. [2]Department of Chemical, Metallurgical and Materials Engineering, Tshwane University of Technology, Pretoria, South Africa. [3]Department of Mechanical Engineering Science, University of Johannesburg, Johannesburg, South Africa. [4]Department of Mechanical Engineering Science, University of Johannesburg, Kingsway Campus, Auckland Park, Johannesburg 2006, South Africa. [5]Department of Metallurgy, Doornfontein Campus, University of Johannesburg, Johannesburg 2028, South Africa.

SN Applied Sciences (2019) 1:85 | https://doi.org/10.1007/s42452-018-0089-5

Received: 26 September 2018 / Accepted: 27 November 2018 / Published online: 7 December 2018

a carbonization step followed by an activation step, while chemical treatment involves impregnation of the precursors with an activating reagent and subsequent heat treatment in an inert environment [9, 10]. Furthermore, the surface morphology of AC also depends on the precursor used. Examples of these precursors are coconut residue, sugarcane bagasse, rice husk, peanut shell, empty fruit bunch, olive oil mill residue, peach stone [9, 11].

The positive influence of temperature during the process of activation is attributed to the enhanced reactivity between the activating agent and carbon at elevated temperature [12]. Furthermore, a rise in surface area and micro-porosity in steam activated olive seeds by increasing the temperature from 700 to 900 °C for about 30 min has been reported [13]. Carbonization at 900 °C for a long period leads to a reduction in surface area and microporosity. Hence, the effect of temperature is very important together with other process parameters like particle size. The influence of heating rate could be unclear because it has a varying influence at different stages of the production of AC. The low heating rate favors the development of porous structure at initial stages of carbonization, while at the last stages, high heating rate is much desired. This is because high heating rate helps to prevent secondary reactions, resulting in a reduction of pore volume [14]. Particle size usually has a significant effect on the carbonization yield of AC due to the slow heating mechanism (slow conduction rate) within large particles, resulting in a reduced volatile release [8]. The finer particle size of an AC enhanced the access to the surface area and the quicker the rate of adsorption kinetics. The heating method is of high importance because the required energy for manufacturing AC is a substantial component of the total production costs [8]. There is a global move in the direction of the generation of renewable energy as the demand for non-renewable coal-based carbon is currently of increasing interest worldwide [15]. In vapor phase systems, finer particle sizes are regarded against pressure drop, which affects energy cost. Thus, a thorough investigation of particle size distribution could provide substantial operating benefits.

Previous works on AC have mostly been tailored towards carbonization of the substrate for efficient adsorptive performance. Even works dated back to the year 2017 have majorly considered the use of separate species [16] for the aforementioned reason and water treatment. Till date, information on the energy consumption in the process of synthesizing AC is scarce. Hence, to bridge this gap in the literature, the most effective way to lower energy consumption while preserving economic development is to determine the energy efficiency during the production of AC. In this regard, this study explored the synthesis of AC from olive seeds, investigating the effect of temperature on the yield, energy efficiency and the dye (methylene blue) removal efficiency of the synthesized ACs. Regression analysis was also used to model how process parameters are related to energy efficiency. Analysis of variance was employed to investigate the influence of carbonization temperature on yield and energy efficiency.

2 Materials and method

2.1 Preparation of activated carbon

The oilseeds were peeled to remove the chaff and then soaked in tap water for 1 h to remove the soft pulp remaining after peeling and then distilled water to remove dirt and residual peels on them. The resulting sample was sun-dried for 1 week and later oven dried at 100 °C for 8 h to remove moisture in them. Subsequently, the dried sample was grounded to powder and sieved into 300 µm particle size for activation. 50 g of the sample was impregnated with 200 ml of H_3PO_4 (14.8 M) solutions. The mixture was left for a period of 24 h before sieving to ensure the acid gain access to the interior of the sample. The acid was sieved out and the sample was dried in an oven at 100 °C for 2 h. After impregnation, the solution was filtered to obtain the residue. The resulting sample was divided into five and carbonized in a conventional stainless-steel electrical furnace at five different temperature level ranging from 600 to 840 °C for 1 h. The effect of temperature on the yield of AC was studied.

2.2 Characterization

The morphological and qualitative analyses of the samples were performed using SEM equipped with EDX. A TESCAN equipped with Oxford instrument X-Max was used for the SEM/EDX analyses. The EDS spectra were obtained by scanning through the surfaces of the samples to determine the elements in the sample.

The phase identification of the samples was carried out using X-Ray Diffraction (Rigaku, Ultima IV). This equipment was used to investigate the diffraction patterns of the AC at a continuous scanning mode.

2.3 Percentage yield of activated carbon

The chemical activation process has a significant influence on the yield of AC. Hence, the yield was determined by dividing the initial mass of the impregnated sample by the final mass of the sample after the whole activation process (Eq. 1)

$$Yield = \frac{W_f}{W_i} \times 100 \quad (1)$$

where W_i is an initial mass of the dry impregnated sample and W_f is the final mass of the sample after carbonization [17].

2.4 Regression analysis

To perform the regression analysis using backward elimination, yields in solid at different temperature for the smallest particle was required—with yield being defined as the amount of AC obtained for a given amount of raw material. Backward elimination method in Minitab starts with all predictors in the model and removes the least significant variable for each step. Then stops when all predictor's variables (temperature and energy efficiency) in the model have *P* values that are less than or equal to the specified Alpha-to-Remove value. By default, the specified Alpha-to-Remove value was 0.1 ($\alpha = 0.1$). Experimental data have shown that temperature affects the yield of AC [18]. Furthermore, experimental data have also shown a linear dependence of yields with temperature [19]. Hence, the yield values obtained experimentally for the temperature and energy efficiency were correlated using linear regression, as expressed by Eq. (2):

$$Yield = -b_0 - b_1 T + b_2 EE \tag{2}$$

where b_1 is the temperature coefficient, b_2 is the energy efficiency coefficient, b_0 is the intercept, T is the temperature and EE, the energy efficiency. Substituting the coefficients b_1, b_2 and b_0 into Eq. (2) by their corresponding values obtained from Minitab 18. The regression model for the yield of olive seed AC is expressed as:

$$Yield = -0.01 - 0.03137T + 0.926EE \tag{3}$$

2.5 Energy efficiency of the furnace

Controlling of the activation temperature is of economic interest, hence in this context, the energy efficiency was done to know the temperature that meets the minimum energy level with the excellent output of activated carbon production from olive seed. The furnace efficiency is obtained from Eqs. 4 and 5.

$$EE = \frac{Energy\ output}{Energy\ input} \times 100 \tag{4}$$

$$EE = \frac{Q_i - Q_{loss}}{Q_i} \times 100 \tag{5}$$

where Heat input$\left(Q_i\right) = \frac{V^2}{R * 4186.8} T$ and $Q_{loss} = \frac{Q}{A}$ [16].

2.6 Adsorption experiments

The batch adsorption was done using 5 sets of 250 mL conical flasks for the five-different temperature range (600 °C, 660 °C, 720 °C, 780 °C, 840 °C). In the adsorption runs, 100 mL of methylene blue (MB) solution with an initial concentration of 100 mg/L was placed in each conical flask. 0.20 g of the prepared AC, with a particle size of 300 µm, was added to the flask and placed in an isothermal shaker at a rotation speed of 120 rpm for 24 h to reach equilibrium. The samples were then filtrated to separate carbon and the residual concentration of MB in the filtrate was analyzed with the aid of UV/visible spectrophotometer. The percentage dye removal from the solution was determined using Eq. 6. Where C_o and C_t are the initial dye concentration and concentration at time, t.

$$\%Removal = \frac{C_0 - C_t}{C_0} \times 100 \tag{6}$$

3 Results

3.1 Characterization

3.1.1 SEM micrograph and determination of pores from threshold image

Figure 1 shows the SEM micrographs of the synthesized AC. All the micrographs clearly show that the AC physical structure consists of cavities on the external surface that enhance porosity. This indicates that the porosity of the substrate improves with an increase in carbonization temperature. Usually, as the temperature increases, devolatilization in turns increases, thereby, developing the basic pore structure in the AC and enhancing the pores to enhance the porosity and higher surface area with fully disordered structures [18]. In addition, the increase in temperature instigated the CO_2 or oxygen in alkali and the surface metal complexes to further gasified the carbon, resulting in pores widening and hence, increasing the pore volume [20] Nonetheless, the control of the carbonization temperature could improve the economic viability of the process since lower temperature with complete activation is usually desired to ensure minimal energy consumption [18].

The pores and interpore spacing within the activated carbon were analyzed for the five-different temperature from scanning electronic microscopy (SEM) images applying threshold image on the SEM images using ImageJ Software. Figure 1 shows that all the synthesized AC are highly porous, having a wide pore size distribution, from visible cracks and crevices of molecular dimensions. Figure 1 reveals that the morphology of the AC produced at 600 °C and 660 °C has structure showing inter-winning dense network with numerous pores and interpore spacing, while the morphology of the

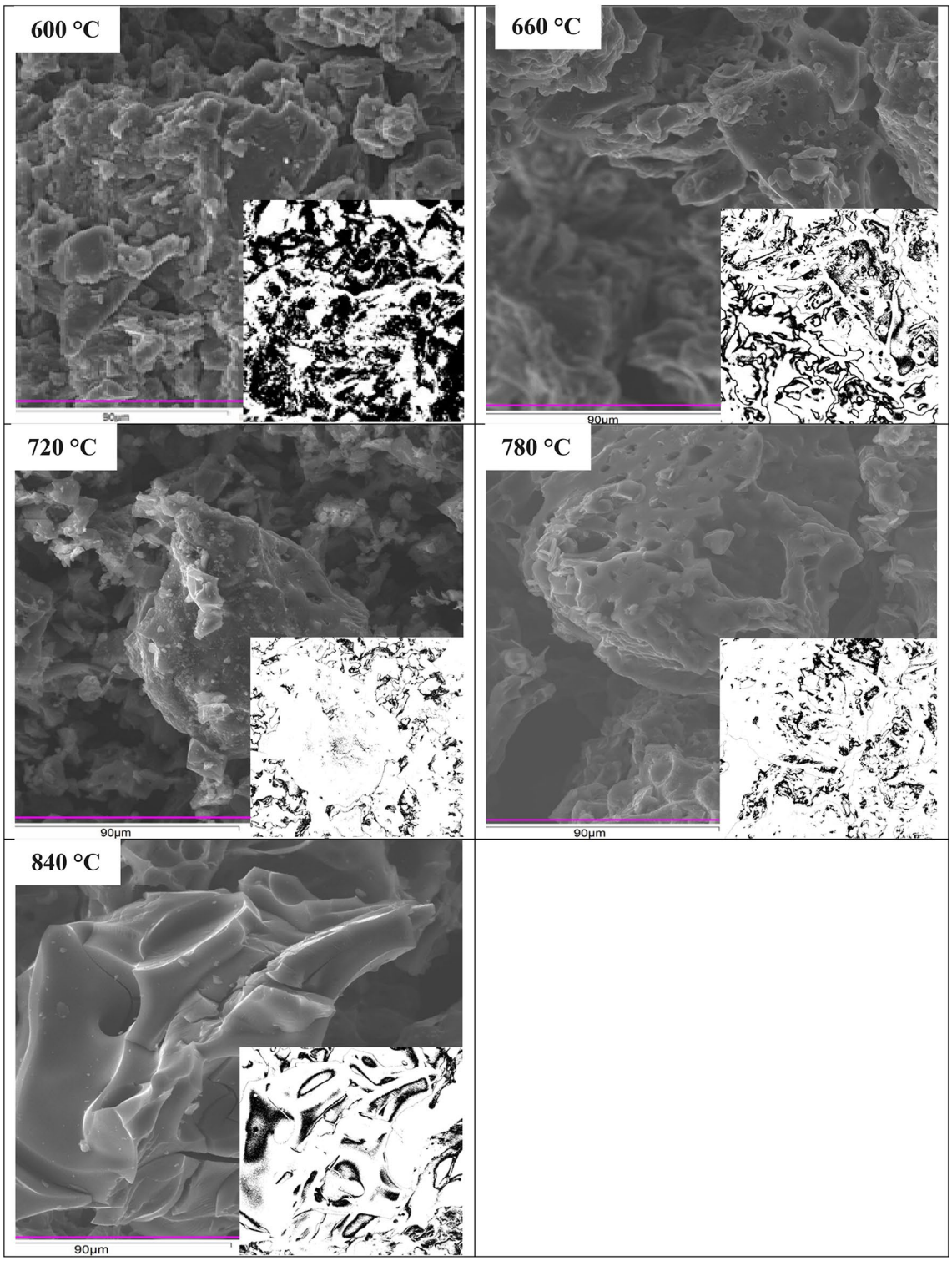

Fig. 1 SEM and threshold image of AC produced from olive seed to identify pores and interpore spacing

AC produced at 720 °C, 780 °C and 840 °C is less dense with transport pores and interpore spacing (Fig. 1). The transport pores in Fig. 1 are the widest pores within the particles, varying from pores greater than 5 molecular diameters to noticeable cracks and crevices, hence, containing a wide variety of different sizes and structural shapes of above 5 orders of magnitude within a single particle of AC [21]. The number of pore decreases with

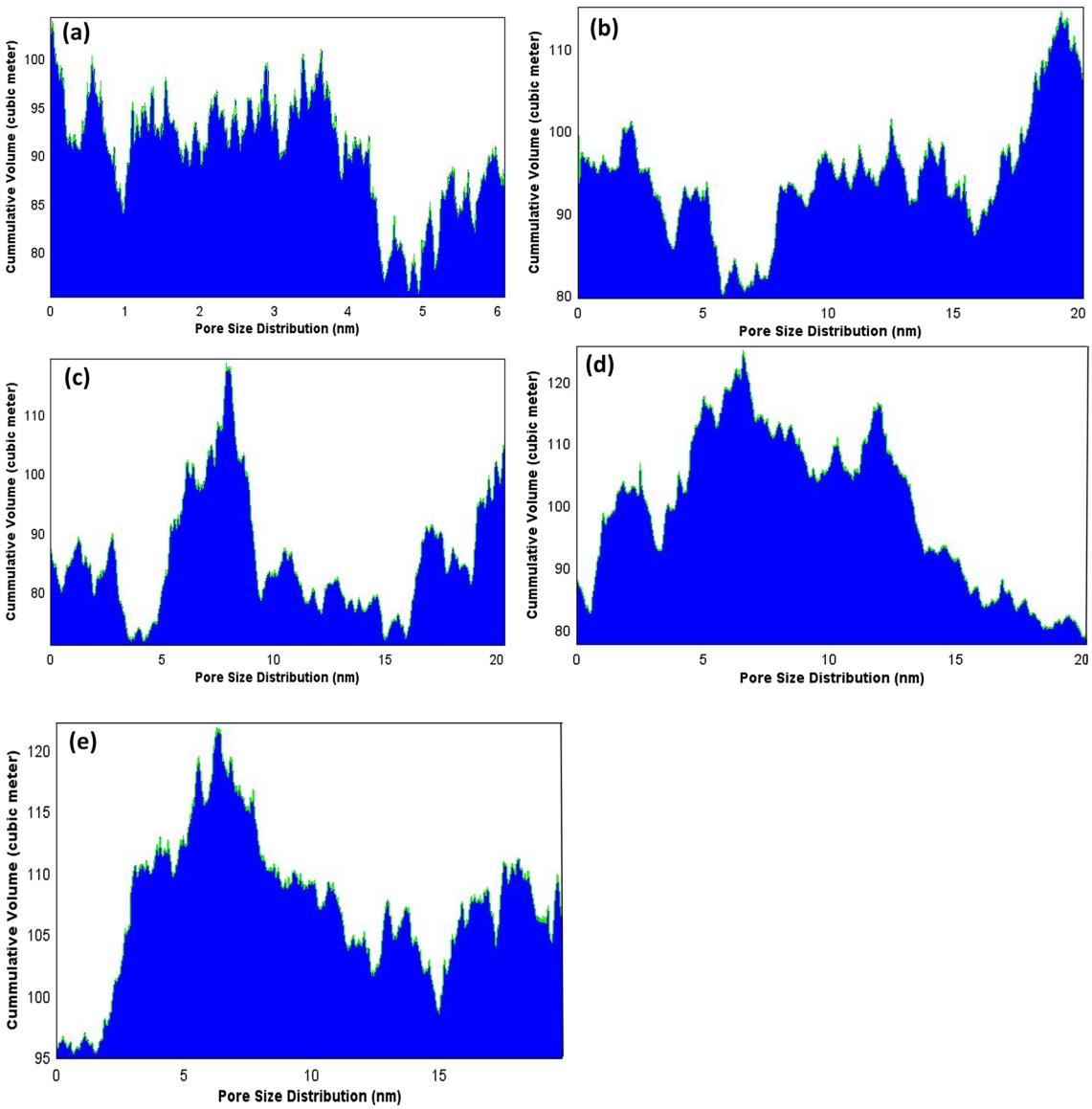

Fig. 2 Pore size distribution at different carbonization temperature **a** 600 °C, **b** 660 °C, **c** 720 °C, **d** 780 °C, **e** 840 °C

increasing temperature, thus, the results confirmed that the yield was influenced by temperature and energy efficiency hence, the pore size of the AC.

3.1.2 Pore size distribution of the activated carbon

Figure 2 presents the pore size distribution of AC signifying the occurrence of micropores and narrow mesopores with broad pore size distribution, however, the level of broadness depends on the carbonization temperature, hence the influence of temperature on AC. As shown in Fig. 2, a high activation temperature brought about a rise in the cumulative pore volume. The variations in the shape of the particle size distribution with an increase in activation temperature reflect changes in the pore structure of AC.

3.1.3 Surface roughness based on the surface plot

The surface roughness of the AC at the five-different temperature (Fig. S1) was measured using the surface plot from ImageJ software. The AC produced at different temperature have a different degree of roughness; the surface roughness at 600–720 °C is high but with lower peak spacing, while the surface roughness at 780–840 °C is low but with high peak spacing. The porous structure is still evident in all the ACs, while the observation at carbonization temperature of 780 °C and 840 °C indicated that the

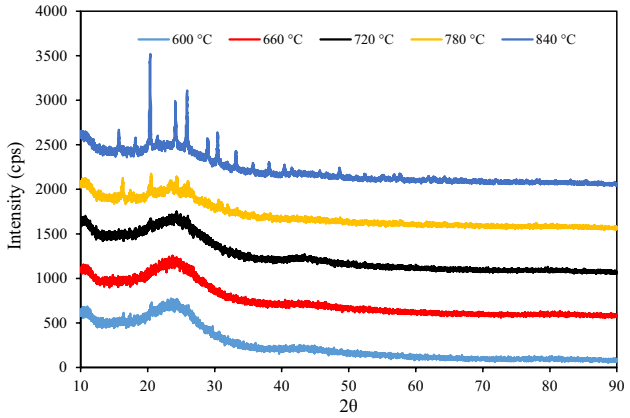

Fig. 3 XRD patterns of representative AC derived from olive seeds at different carbonization temperature

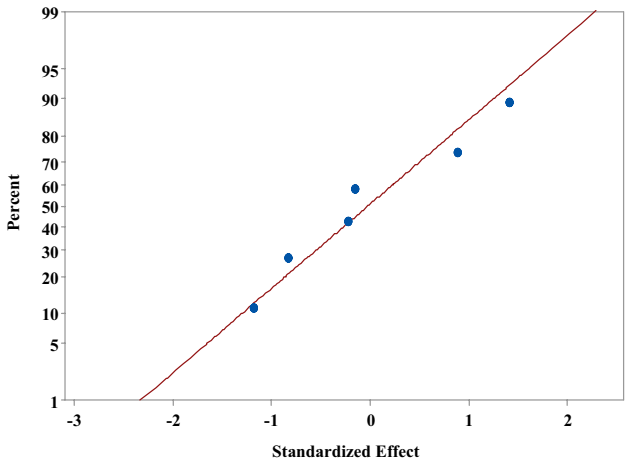

Fig. 4 Normal probability plot of standardized effects

obtained ACs have cracks probably originated from the increase in temperature.

3.1.4 X-ray diffraction analysis

Figure 3 shows microcrystalline bands of random alignment imposed by the roughness of the substrate (Fig. S1). The diffraction profiles exhibit two prominent broad bands for carbonization temperature of 600 °C, 660 °C and 720 °C centered around 2θ = 24° and 43° with a crystalline size between 30 and 35 (A) and strain between 07 and 09% (Fig. 3a–c). The two broad bands showed the presence of an amorphous structure that is not orderly stacked up by carbon rings and could help to produce a well-defined adsorbent [22]. The XRD pattern of AC at a higher temperature of 780 °C and 840 °C is quite different where the two broad bands vanished and some tiny bands emerged (Fig. 3d, e). The higher carbonization temperature of 780 °C and 800 °C, goes together with a general and gradual change evident by an increase in sharpness of bands around 2θ = 10°, 18°, 20°, 24°, 30°, 33°, 35°, 38°, 40°, 48°, 55° and 62°. This observation at a carbonization temperature of 780 °C and 800 °C revealed that the structure synthesized ACs is fully disordered (see Figs. 1 and S1). This is due to the presence of planer defects, which characterizes the disordering of crystallographic planes because of random shifts between adjacent layers. The high angular bands (50°–62°) are more diffuse and broad with much lower diffraction. However, from the XRD analysis of ACs, undefined patterns observed increase with an increase in activation temperature. This could be because of the crystal structure of compounds of unlike atoms, which is built up on the skeleton of a Bravais lattice [23].

3.2 Effect of temperature on the stability of elements

Elemental stability in the context of this study is the resistance of the elements to the rays of scanning electron microscopy in detecting the elements present the AC at different carbonization temperature. If the elements are stable, the rays of the microscope will detect them. SEM/EDX can examine the internal structure of materials and the capacity to give an elemental analysis of the specimen, by utilizing the swift variations of atomic number and absorption coefficient with wavelength. The elemental analysis of the AC study is shown in Fig. S2. The presence of Tungsten at a temperature of 600–720 °C (Figs. S2a–S2c) is due to the presence of an activating agent, which confined the oxidation temperature within the limit of 600–720 °C, though the normal oxidation temperature of Tungsten ranges from 400 to 900 °C [23]. The combined ripple effect of the activation agent and the temperature of AC causes Tungsten to be resistant to heat at a temperature range of 780–840 °C, hence, Tungsten was lost at this temperature (Fig. S2e). Phosphorous, potassium, oxygen, calcium, sodium, and aluminum in olive seeds have strong affinity at all temperature, hence a strong degree of combining with each other (see Fig. S2a–S2e). Iron was not visible at all temperature except at 720 °C, this could own to the fact that other element overlaps it, as they serve as barriers to the rays.

Furthermore, the macroscopic elements in the AC can be deduced from the angles between the faces of a well-developed crystal in the XRD patterns (Fig. 3), without any knowledge of the atom arrangement inside the crystal. Hence, undefined patterns observed with an increase in activation temperature is related to some metal impurity in EDX analysis because of the crystal structure of compounds of unlike atoms. These impurities might be an ordinary

Table 1 The analysis of variances for the AC yield

Source	DF	Seq SS	Contribution (%)	Adj SS	Adj MS	*F* value	*P* value
Regression	2	5041.86	99.35	5041.86	2520.93	228.79	0.001
Temperature °C	1	4420.31	87.10	185.78	185.78	16.86	0.026
Energy efficiency	1	621.55	12.25	621.55	621.55	56.41	0.005
Error	3	33.06	0.65	33.06	11.02		
Total	5	5074.91	100.00				

Table 2 Model summary

S	R^2	R^2(adj)	Press	R^2 (pred)
3.31942	99.35%	98.91%	1625724901	0.00%

chemical compound or an intermediate phase of relatively fixed composition in the ACs, or an ordered solid solution [23].

3.3 Regression analysis, normal probability plot and residual analysis

The analysis of variance was investigated at 95% significance level, based on the sequential sum of squares (Seq SS), the degree of freedom (DF), adjusted mean squares (Adj MS), adjusted sun squares (Adj SS), F values and *P* values of the predictors as shown in Table 1. Table 2 gives the model summary with R^2 of 99.35% and the coefficients of parameters are shown in Table 3. The determination (R^2) of the model implies that 99.35% of the variations in yield can be explained by the independent variables while only 0.65% of variations cannot be explained by the model. The parameters with high *T* values and *P* values less than 0.1 (Alpha-to-Remove value) are indicative of relevant factors [24]. This indicates that the postulation being irrelevance (null hypothesis) must be rejected for that parameter to give high variance by any changes in that specific parameter [8]. From all these analyses, activation temperature selected from the Mintab 18 is the most significant process factor, with 87.10% contribution to the carbonization process. This in turns influenced the Energy efficiency with 12.5%, as the contribution to the carbonization process.

To assess the distribution status of the experimental data set, the normal probability plot of the effects was investigated, and it reveals the standardized effects relative to a distribution fit line. The normal probability plot of the standardized effect obtained is shown in Fig. 4. Plotted points falling along an imaginary straight line indicated the estimated effects of the temperature and energy efficiency since the points on the plot fall close to a straight line, which is traceable to the normal random variability. While the plotted points falling far away from the imaginary line at the upper right and lower left corners of the plot, indicated projected influences that could be significant statistically. Thus, the selected model successfully reveals how closely the set of observed values match the theoretical distribution. The acceptability of the model was assessed by the standardized residuals (the difference between the predicted and the experimental values). Residuals are believed to be elements of variation unexplained by the fitted model and it is then expected that they occur according to a normal distribution [25] (Fig. 4). The yield predicted versus the standard residual is shown in Fig. 5. All the points were found to fall in the range of + 1.4 to − 1.4, which shows that the model presents a minimal deviation from the fitted value from the observed value [26, 27].

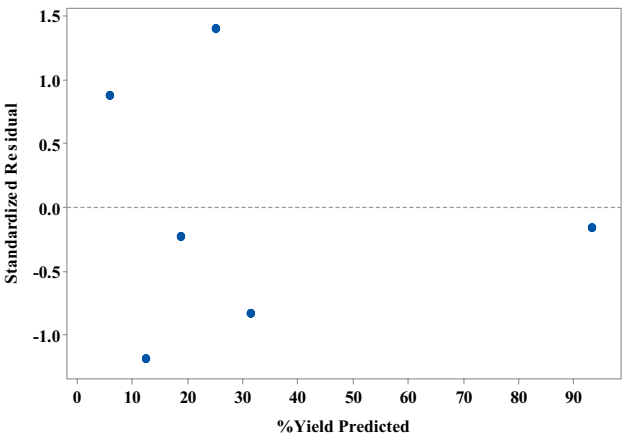

Fig. 5 Standardized residual versus percentage yield (predicted)

Table 3 Coefficients of parameters

Term	Coef	SE Coef	95% CI	*T* value	*P* value	VIF
Constant	− 0.01	2.03	(− 6.47, 6.47)	− 0.01	1.000	
Temperature °C	− 0.03137	0.00764	(− 0.05568, − 0.00706)	− 4.11	0.026	36.80
energy Efficiency	0.926	0.123	(0.534, 1.318)	7.51	0.005	36.80

3.4 Relationship between temperature and energy efficiency

Energy use in the production of AC is significantly influenced by temperature, hence the impact of energy efficiency on yield depend on the level of temperature. Thermal property is temperature dependent and its reciprocal is thermal resistivity and the energy efficiency of AC which bears an inverse relationship to its temperature. Figure 6 shows that the higher the temperature, the lower the energy efficiency. This is because more heat is lost at higher temperatures. This also ensures a constant and instantaneous match between the AC yield and the energy efficiency required for producing AC at a yield and a temperature profile. Table 4 gives the variation of temperature and the calculated heat input and heat output used for the energy efficiency (EE).

3.5 Influence of activation temperature on AC yield

Figure 7 presents the effect of activation temperature on the yield of AC. The yield of AC decreases from 31 to 7% with increasing temperature from 600 to 840 °C similar to the report of [28]. This result is better than the result reported by [11] when they produced AC from coconut residue. Cazetta et al. [28] reported that the yield is influenced by the ratio of the activating agent to char. In this study, H_3PO_4 and electricity were the major factors responsible for most of the impacts in the synthesis of AC [29]. High carbonization temperature has a disadvantage, the yield of AC could be low due to the carbon removal with H and O (as COx and hydrocarbons) [18] and assessing the energy efficiency of AC production has the potential to save and improve energy security. The AC yield significantly decreased with higher carbonization temperature and increased with at higher energy efficiency (Fig. 7) with respect to lower temperature. Hence, concluded that the higher yield was achieved at a lower temperature and higher energy efficiency, which will result in the decrease in the cost of producing AC. The reduction of yield with respect to activation temperature is most likely not only because of the completeness of the carbonization and volatilization process but also because of certain combustion at higher temperatures since the process occurred in the presence of air [30]. It was observed that predicted values conform closely experimental for the energy efficiencies of the AC formed from the olive seeds. The agreement between the predicted and experimental data can be seen in their equations which are similar except for the R-square values which show a percent deviation of 7–8% (see Fig. 7).

Table 4 Variation of temperature on energy efficiency

Samples	Temperature (°C)	Heat input (W/m^{2}K)	Heat loss (W/m^{2}K)	eE
1	600	1375.75	630.37	54.18
2	660	1375.75	696.68	49.36
3	720	1375.75	763.13	44.53
4	780	1375.75	829.44	39.71
5	840	1375.75	895.89	34.88

3.6 Adsorption capacity for methylene blue

Table 5 gives the adsorption capacity for dye removal experiments. The dye removal capacity of the synthesized activated carbon in this study is similar to that reported by Cazetta et al. [28] and Li et al. [31]. The adsorption capacity of the adsorbent increased with increase in the temperature of the system from 600 to 720 °C as shown in Table 5. The percentage of adsorption at this temperature range

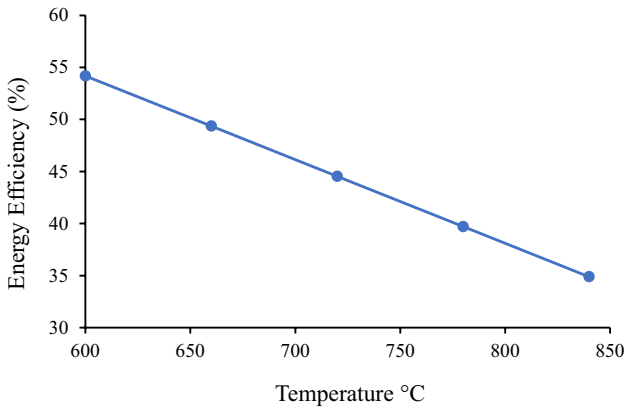

Fig. 6 Energy efficiency versus temperature

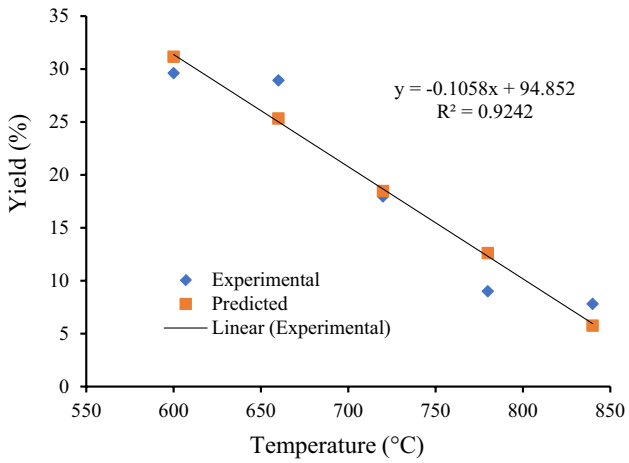

Fig. 7 Influence of activation temperature and energy efficiency on yield

Table 5 Dye removal efficiency using AC produced from olive seed at different temperature

Temperature (°C)	Dye removal efficiency (%)
600	96.4
660	96.9
720	97.5
780	95.3
840	95.3

increases with rising temperature, demonstrating that the adsorption process at this temperature range is endothermic [32]. It was observed that the adsorption capacity of the adsorbent slightly reduced at 780–840 °C from 97.5 to 95.3% with constant % dye removal, hence, the optimum temperature and the optimum EE for the removal of dye using olive seeds produced AC is 600 °C and 44.53% respectively.

4 Conclusion

Yield and Energy consumption are the essential factors to consider during the production of AC. This investigation was done to elucidate the effect of carbonization temperature during the production of AC on the energy efficiency and yield of the AC produced from olive seeds. Carbonization temperature has a strong effect on the energy efficiency and yield of AC produced. Lower heat treatment (temperature) reduces the consumption of energy without penalizing the yield. The pore structure, surface roughness and elements found in the AC were strongly affected by carbonization temperature. The optimum temperature for dye removal using AC produced from olive seeds is 600 °C, exhibiting a removal efficiency of 96.4%.

Compliance with ethical standards

Conflict of interest The authors declare that they have no conflict of interest.

References

1. Gurten II, Ozmak M, Yagmur E, Aktas Z (2012) Preparation and characterization of activated carbon from waste tea using K_2CO_3. Biomass Bioenerg 37:73–81. https://doi.org/10.1016/j.biombioe.2011.12.030
2. Shiono T, Yamamoto K, Yotsumoto Y, Yoshida A (2017) Caffeine adsorption of montmorillonite in coffee extract. Biosci, Biotechnol Biochem 81:1591–1597. https://doi.org/10.1080/09168451.2017.1340087
3. Alaba PA, Oladoja NA, Sani YM, Ayodele OB, Mohammed IY, Olupinla SF, Daud WMW (2018) Insight into wastewater decontamination using polymeric adsorbents. J Environ Chem Eng 6:1651–1672. https://doi.org/10.1016/j.jece.2018.02.019
4. Alaba PA, Sani YM, Olupinla SF, Daud WMW, Mohammed IY, Enweremadu CC, Ayodele OO (2017) Toward *N*-nitrosamines free water: formation, prevention, and removal. Crit Rev Environ Sci Technol 47(24):2448–2489. https://doi.org/10.1080/10643389.2018.1430438
5. Zhang Y, Campbell R, Drake M, Zhong Q (2015) Decolorization of Cheddar cheese whey by activated carbon. J Dairy Sci 98:2982–2991. https://doi.org/10.3168/jds.2014-9159
6. Hu S-H, Shiue A, Chang S-M, Chang Y-T, Tseng C-H, Mao C-C, Hsieh A, Chan A (2016) Removal of carbon dioxide in the indoor environment with sorption-type air filters. Int J Low-Carbon Technol 12(3):330–334. https://doi.org/10.1093/ijlct/ctw014
7. Arena N, Lee J, Clift R (2016) Life cycle assessment of activated carbon production from coconut shells. J Clean Prod 125:68–77. https://doi.org/10.1016/j.jclepro.2016.03.073
8. Sharifan SA (2013) Comparative optimisation study of activated carbon production from hazelnut shells by thermal and microwave heating methods. Dissertation, Imperial College London
9. Yahya MA, Al-Qodah Z, Ngah CWZ (2015) Agricultural bio-waste materials as potential sustainable precursors used for activated carbon production: a review. Renew Sustain Energy Rev 46:218–235. https://doi.org/10.1016/j.rser.2015.02.051
10. Yahya MA, Ngah CWZCW, Hashim MA, Al-Qodah Z (2016) Preparation of activated carbon from desiccated coconut residue by chemical activation with NaOH. J Mater Sci Res 5(1):24–31
11. Yahya MA, Al-Qodah Z, Ngah C, Hashim MA (2015) Preparation and characterization of activated carbon from desiccated coconut residue by potassium hydroxide. Asian J Chem 27(6):2331–2336. https://doi.org/10.14233/ajchem.2015.18804
12. Bhatnagar A, Kaczala F, Hogland W, Marques M, Paraskeva CA, Papadakis VG, Sillanpää M (2014) Valorization of solid waste products from olive oil industry as potential adsorbents for water pollution control—a review. Environ Sci Pollut Res 21(1):268–298. https://doi.org/10.1007/s11356-013-2135-6
13. Alabadi A, Razzaque S, Yang Y, Chen S, Tan B (2015) Highly porous activated carbon materials from carbonized biomass with high CO_2 capturing capacity. Chem Eng J 281:606–612. https://doi.org/10.1016/j.cej.2015.06.032
14. Abioye AM, Ani FN (2015) Recent development in the production of activated carbon electrodes from agricultural waste biomass for supercapacitors: a review. Renew Sustain Energy Rev 52:1282–1293. https://doi.org/10.1016/j.rser.2015.07.129
15. Ahmed MJ (2016) Application of agricultural based activated carbons by microwave and conventional activations for basic dye adsorption. J Environ Chem Eng 4(1):89–99. https://doi.org/10.1016/j.jece.2015.10.027
16. Sanni ES, Emetere ME, Odigure JO, Efeovbokhan VE, Agboola O, Sadiku ER (2017) Determination of optimum conditions for the production of activated carbon derived from separate varieties of coconut shells. Int J Chem Eng 2017:1–16. https://doi.org/10.1155/2017/2801359
17. Anisuzzaman SM, Joseph CG, Daud ABW, Krishnaiah D, Yee HS (2015) Preparation and characterization of activated carbon from Typha orientalis leaves. Int J Ind Chem 6:9–21. https://doi.org/10.1007/s40090-014-0027-3
18. Joshi RR (2015) Optimization of conditions for the preparation of activated carbon from Lapsi (*Choerospondias axillaris*) seed stone using $ZnCl_2$. J Inst Eng 11:128–139. https://doi.org/10.3126/jie.v11i1.14707
19. Otulana JO, Oluwole OO, Adeleke MB (2016) A rector plant for activated carbon production. Int J Novel Res Eng Sci 2:20
20. Adebisi GA, Chowdhury ZZ, Alaba PA (2017) Equilibrium, kinetic, and thermodynamic studies of lead ion and zinc ion adsorption from aqueous solution onto activated carbon prepared from

palm oil mill effluent. J Clean Prod 148:958–968. https://doi.org/10.1016/j.jclepro.2017.02.047
21. Callewaert J (2014) Activated carbon pores. DESOTEC Activated Carbon. https://www.desotec.com/en/carbonology/carbonology-cases/activated-carbon-pores. Assessed 21 May 2014
22. Tang Y-B, Liu Q, Chen F-Y (2012) Preparation and characterization of activated carbon from waste ramulus mori. Chem Eng J 203:19–24. https://doi.org/10.1016/j.cej.2012.07.007
23. Nilsson C, Habainy J (2013) Oxidation of pure tungsten in the temperature interval 400° to 900 °C. Diploma work
24. Danish M, Hashim R, Ibrahim MNM, Sulaiman O (2014) Optimized preparation for large surface area activated carbon from date (*Phoenix dactylifera* L.) stone biomass. Biomass Bioenergy 61:167–178
25. Hegazy AK, Abdel-Ghani NT, El-Chaghaby GA (2014) Adsorption of phenol onto activated carbon from *Rhazya stricta*: determination of the optimal experimental parameters using factorial design.". Appl Water Sci 4(3):273–281
26. Hamdon A, Azza A, Darwish NA, Hilal N (2015) The use of factorial design in the analysis of air-gap membrane distillation data. Desalination 367:90–102
27. Hegazy AK, Abdel-Ghani NT, El-Chaghaby GA (2014) Adsorption of phenol onto activated carbon from *Rhazya stricta*: determination of the optimal experimental parameters using factorial design. Appl Water Sci 4(3):273–281. https://doi.org/10.1007/s13201-013-0143-9
28. Cazetta AL, Vargas AM, Nogami EM, Kunita MH, Guilherme MR, Martins AC, Silva TL, Moraes JC, Almeida VC (2011) NaOH-activated carbon of high surface area produced from coconut shell: kinetics and equilibrium studies from the methylene blue adsorption. Chem Eng J 174(1):117–125. https://doi.org/10.1016/j.cej.2011.08.058
29. Hjaila K, Baccar R, Sarrà M, Gasol CM, Blánquez P (2013) Environmental impact associated with activated carbon preparation from olive-waste cake via life cycle assessment. J Environ Manag 130:242. https://doi.org/10.1016/j.jenvman.2013.08.061
30. Hao W, Björkman E, Lilliestråle M, Hedin N (2014) Activated carbons for water treatment prepared by phosphoric acid activation of hydrothermally treated beer waste. Ind Eng Chem Res 53(40):15389–15397. https://doi.org/10.1021/ie5004569
31. Li Y, Qiuju D, Liu T, Peng X, Wang J, Sun J, Wang Y et al (2013) Comparative study of methylene blue dye adsorption onto activated carbon, graphene oxide, and carbon nanotubes. Chem Eng Res Des 91(2):361–368. https://doi.org/10.1016/j.cherd.2012.07.007
32. Hayeeye F, Sattar M, Tekasakul S, Sirichote O (2014) Adsorption of Rhodamine B on activated carbon obtained from pericarp of rubber fruit in comparison with the commercial activated carbon. Songklanakarin J Sci Technol 36(2):177–187